Correction

NEUROSCIENCE

Correction for "Sympathetic innervation controls homeostasis of neuromuscular junctions in health and disease," by Muzamil Majid Khan, Danilo Lustrino, Willian A. Silveira, Franziska Wild, Tatjana Straka, Yasmin Issop, Emily O'Connor, Dan Cox, Markus Reischl, Till Marquardt, Dittmar Labeit, Siegfried Labeit, Evelyne Benoit, Jordi Molgó, Hanns Lochmüller, Veit Witzemann, Isis C. Kettelhut, Luiz C. C. Navegantes, Tullio Pozzan, and Rüdiger Rudolf, which appeared in issue 3, January 19, 2016, of *Proc Natl Acad Sci USA* (113:746–750; first published January 5, 2016; 10.1073/pnas.1524272113).

The authors note that the following statement should be added to the Acknowledgments: "T.M. was supported by European Research Council (ERC) Grant Agreement 311710-MU TUNING of the European Union's Seventh Framework Programme (FP/2007-2013)."

www.pnas.org/cgi/doi/10.1073/pnas.1708559114

Sympathetic innervation controls homeostasis of neuromuscular junctions in health and disease

Muzamil Majid Khan[a,b,c], Danilo Lustrino[d,e], Willian A. Silveira[d,e], Franziska Wild[a,b,c], Tatjana Straka[a,b,c], Yasmin Issop[f], Emily O'Connor[f], Dan Cox[f], Markus Reischl[g], Till Marquardt[h], Dittmar Labeit[i], Siegfried Labeit[i], Evelyne Benoit[j,k], Jordi Molgó[j,k], Hanns Lochmüller[f], Veit Witzemann[l], Isis C. Kettelhut[d,e], Luiz C. C. Navegantes[d,e], Tullio Pozzan[m,n,1], and Rüdiger Rudolf[a,b,c,1,2]

[a]Interdisciplinary Center for Neurosciences, Universität Heidelberg, 69120 Heidelberg, Germany; [b]Institute of Molecular and Cell Biology, Hochschule Mannheim, 68163 Mannheim, Germany; [c]Institute of Toxicology and Genetics, Karlsruhe Institute of Technology, 76344 Eggenstein-Leopoldshafen, Germany; [d]Department of Physiology, Faculdade de Medicina de Ribeirão Preto, University of São Paulo, 14049-900 Ribeirão Preto, Brazil; [e]Department of Biochemistry and Immunology, Faculdade de Medicina de Ribeirão Preto, University of São Paulo, 14049-900 Ribeirão Preto, Brazil; [f]The John Walton Muscular Dystrophy Research Centre, Medical Research Council Centre for Neuromuscular Diseases, Newcastle University, Newcastle upon Tyne NE1 3BZ, United Kingdom; [g]Institute of Applied Informatics, Karlsruhe Institute of Technology, 76344 Eggenstein-Leopoldshafen, Germany; [h]Developmental Neurobiology Laboratory, European Neuroscience Institute, 37077 Göttingen, Germany; [i]Department of Integrative Pathophysiology, Universität Heidelberg, 68167 Mannheim, Germany; [j]Commissariat a l'energie atomique, Institut de Biologie et Technologies de Saclay (iBiTec-S), Service d'Ingénierie Moléculaire des Protéines (SIMOPRO), 91191 Gif-sur-Yvette Cedex, France; [k]Institut des Neurosciences Paris-Saclay, UMR 9197, CNRS/Université Paris-Sud, 91190 Gif-sur-Yvette Cedex, France; [l]Max Planck Institute for Medical Research, 69120 Heidelberg, Germany; [m]Department of Biomedical Sciences, University of Padua, 35121 Padua, Italy; and [n]Institute of Neuroscience, Padua Section, National Research Council, 35121 Padua, Italy

Contributed by Tullio Pozzan, December 11, 2015 (sent for review November 10, 2015; reviewed by Frederic A. Meunier and Antonio Musaro)

The distribution and function of sympathetic innervation in skeletal muscle have largely remained elusive. Here we demonstrate that sympathetic neurons make close contact with neuromuscular junctions and form a network in skeletal muscle that may functionally couple different targets including blood vessels, motor neurons, and muscle fibers. Direct stimulation of sympathetic neurons led to activation of muscle postsynaptic β2-adrenoreceptor (ADRB2), cAMP production, and import of the transcriptional coactivator peroxisome proliferator-activated receptor γ-coactivator 1α (PPARGC1A) into myonuclei. Electrophysiological and morphological deficits of neuromuscular junctions upon sympathectomy and in myasthenic mice were rescued by sympathicomimetic treatment. In conclusion, this study identifies the neuromuscular junction as a target of the sympathetic nervous system and shows that sympathetic input is crucial for synapse maintenance and function.

neuromuscular junction | sympathetic neurons | cAMP | beta-agonists | myasthenia

With the exception of the regulation of blood vessel smooth muscle tonus, functions of sympathetic neurons in skeletal muscle have scarcely been explored (1, 2). Recently, sympathicomimetics (SM) have been introduced successfully as clinical treatment of neuromuscular transmission disorders called congenital myasthenic syndromes (CMSs) (3, 4). Fittingly, muscle weakness is a hallmark of several autonomous nervous system disorders, including chronic fatigue syndrome (5), congenital insensitivity to pain (6), adrenal insufficiency (7, 8), complex regional pain syndromes (9, 10), and Lambert–Eaton myasthenic syndrome (11–13). Because, furthermore, beta-blockers lead to increased susceptibility to muscle fatigue (14) and modulate neuromuscular activity of drugs applied during anesthesia (15), we became interested in addressing sympathetic innervation of skeletal muscle.

Results

A Network of Sympathetic Neurons Contacts Different Targets in Skeletal Muscle. To investigate the distribution of sympathetic neurons in mouse skeletal muscle, we used reporter mice expressing Tomato protein under control of the dopamine β-hydroxylase (DBH) promoter (16) (DBH-Tomato). Tomato colocalized with immunofluorescence (IF) signals of the sympathetic markers tyrosine hydroxylase (TH) (Fig. 1*A*) and neuropeptide Y (Fig. S1). Sympathetic neurons were present in large amounts throughout the diaphragm muscle (Fig. 1*A* and Fig. S1*A*). Axons either innervated or passed in proximity to neuromuscular junctions (NMJs) that were stained with fluorescent alpha-bungarotoxin conjugate (BGT-AF647) (Fig. 1*A* and Fig. S1). Costaining of extensor digitorum longus (EDL) muscles with wheat germ agglutinin (WGA), TH antibody, and BGT-AF647 showed that TH-positive axons were associated with blood vessels (Fig. S2). However, 69.86 ± 11.22% (mean ± SEM, $n = 5$) NMJ regions also displayed plaque-like TH immunosignals, which connected to TH-immunopositive axons. The cholinergic presynaptic marker vesicular acetylcholine transporter (VACHT) perfectly colocalized with AChRs but only partially with TH (Fig. 1*B*); 67.59 ± 8.83% (mean ± SEM, $n = 10$) of VACHT-positive portions of motor neuron axons (Fig. 1*B*, open arrowheads) were accompanied by TH-positive axons, which then formed connections to other TH-positive axons (Fig. 1*B*, asterisks). Muscle transverse sections stained with anti-TH antibody and BGT demonstrated that 95.8 ± 2.6% and 90.6 ± 1.96% (both mean ± SEM, $n = 4$) of NMJ regions were TH-immunopositive in EDL and soleus muscles, respectively (Fig. 1*D*).

Significance

The sympathetic nervous system regulates basic body functions such as heartbeat, blood pressure, and gland activities. Whereas hormone secretion from the adrenal medulla modulates these processes systemically, local and fast responses can be mediated by direct sympathetic innervation. Although many effects of the sympathetic system on skeletal muscle physiology and disease are known, direct sympathetic innervation targets in skeletal muscle have been scarcely studied. We investigated this aspect and found that neuromuscular junctions, the contact points between motor neurons and muscle fibers, are innervated by sympathetic neurons, which is of crucial importance for the integrity and function of nerve–muscle contact. Our findings help to understand and refine treatment of neuromuscular diseases, including myasthenic syndromes.

Author contributions: M.M.K., D. Lustrino, W.A.S., J.M., H.L., V.W., I.C.K., L.C.C.N., T.P., and R.R. designed research; M.M.K., D. Lustrino, W.A.S., F.W., T.S., Y.I., E.O., D.C., E.B., J.M., and R.R. performed research; D. Lustrino, T.M., D. Labeit, S.L., and V.W. contributed new reagents/analytic tools; M.M.K., D. Lustrino, W.A.S., F.W., Y.I., E.O., D.C., M.R., and R.R. analyzed data; and M.M.K., H.L., L.C.C.N., T.P., and R.R. wrote the paper.

Reviewers: F.A.M., The University of Queensland; and A.M., Sapienza University of Rome.

The authors declare no conflict of interest.

[1]To whom correspondence may be addressed. Email: tullio.pozzan@unipd.it or r.rudolf@hs-mannheim.de.

[2]Present address: Hochschule Mannheim, Institute of Molecular and Cell Biology, 68163 Mannheim, Germany.

This article contains supporting information online at www.pnas.org/lookup/suppl/doi:10.1073/pnas.1524272113/-/DCSupplemental.

www.pnas.org/cgi/doi/10.1073/pnas.1524272113

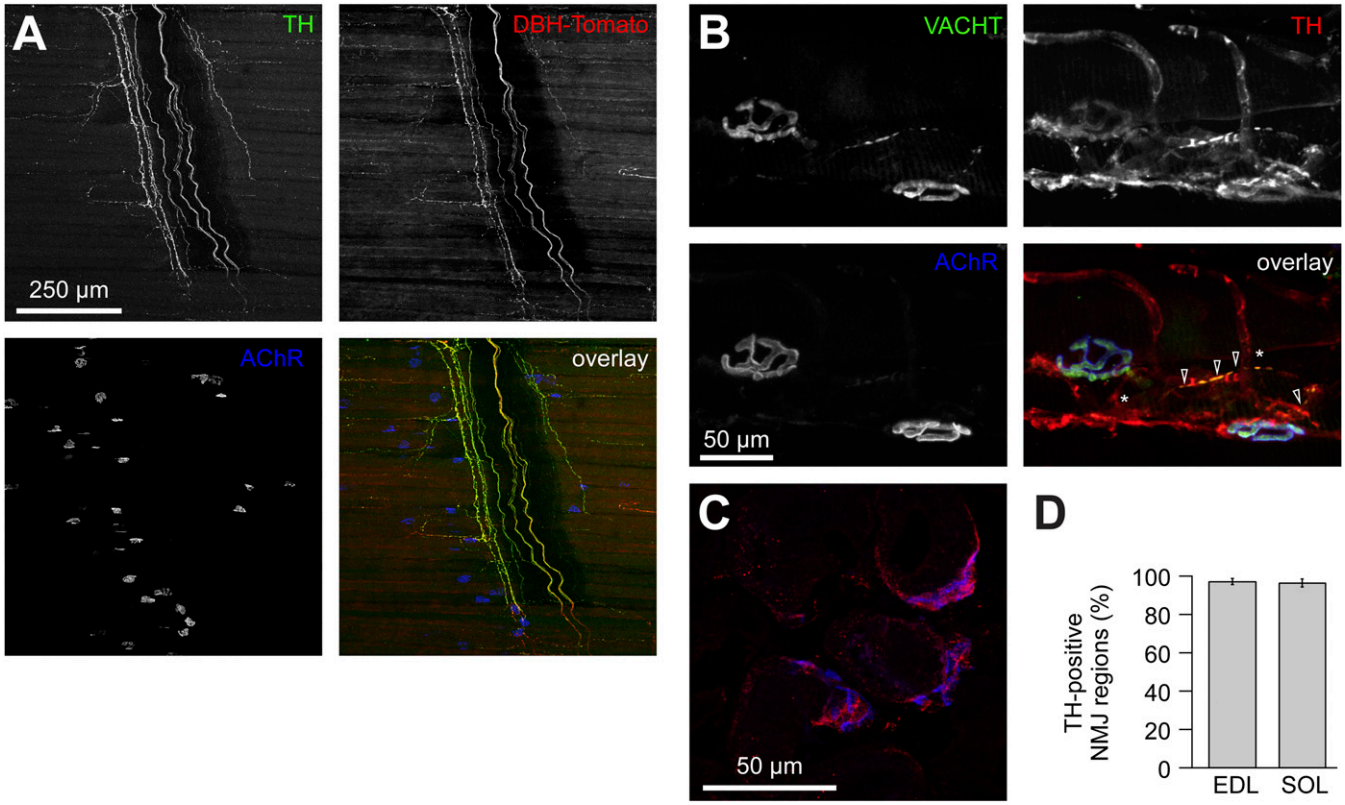

Fig. 1. Distribution of sympathetic neurons in skeletal muscle. (*A*) Diaphragm muscle of a DBH-Tomato mouse expressing Tomato protein in sympathetic neurons was costained with anti-TH antibody and BGT-AF647 (AChR). Signals from TH, Tomato, and BGT are depicted in the overlay in green, red, and blue, respectively. Three-dimensional maximum projection of a confocal z stack of a representative region is shown. All channels were brightness/contrast-enhanced. (*B*) Longitudinal sections of wild-type EDL muscles were labeled against VACHT, TH, and BGT-AF647. Signals from these markers are depicted in the overlay in green, red, and blue, respectively. Three-dimensional maximum projection of a confocal z stack of a representative region is shown. All channels were brightness/contrast-enhanced. (*C* and *D*) EDL and soleus muscles were sectioned transversally, stained with BGT-AF555 (blue in overlay) and anti-TH antibody (red in overlay), and then imaged with confocal microscopy. (*C*) Representative confocal brightness/contrast-enhanced optical section from EDL. (*D*) Quantification of TH-positive NMJ regions from EDL and soleus (SOL) muscles. Mean ± SEM (n = 4 muscles each). Negative controls lacking primary antibodies showed 0.7 ± 0.7% (mean ± SEM, n = 4 muscles) in EDL and 0.0% (mean ± SEM, n = 4 muscles) in soleus of TH-positive NMJ regions.

Functional Effects of Sympathetic Stimulation on Muscle and NMJs. The most abundant targets of norepinephrine in skeletal muscle are β2-adrenoreceptors (ADRB2s) (17, 18). Transverse sections of EDL were stained for ADRB2s and AChRs. Colocalization analysis showed a Pearson's coefficient of 0.70 ± 0.04 (mean ± SEM, n = 13; Fig. S3 *A* and *B*), suggesting enrichment of ADRB2 in the NMJ. Sympathetic neuron activity on postsynaptic ADRB2 signaling was tested using the Förster resonance energy transfer (FRET)-based

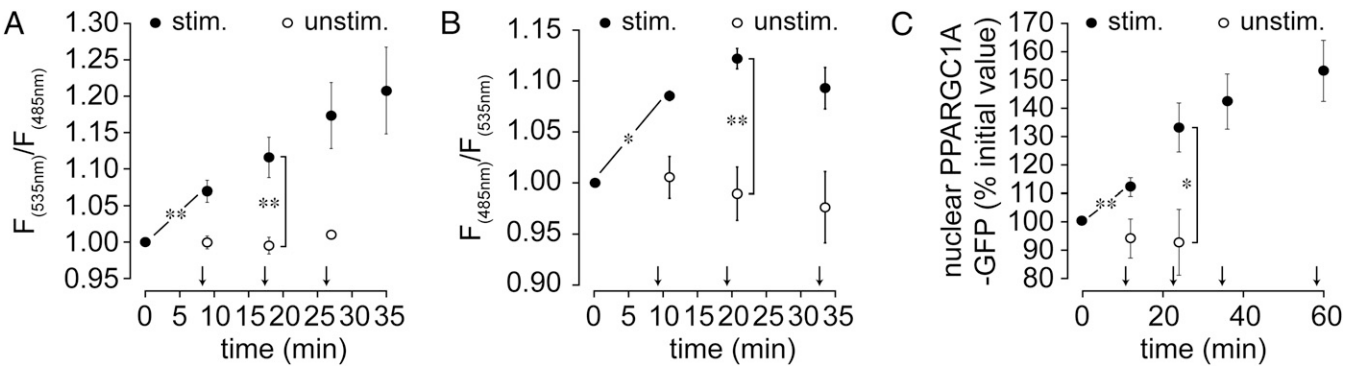

Fig. 2. Stimulation of the lumbar sympathetic ganglion stimulates muscle adrenergic signal transduction and nuclear import of PPARGC1A. TA muscles were transfected with β2-AR-s-pep (*A*), RAPSN-EPAC (*B*), or PPARGC1A-GFP (*C*). Ten days later, muscles were injected with BGT-AF647 to label NMJs and imaged with in vivo confocal and two-photon microscopy. (*A* and *B*) Quantification of FRET measurements. Graphs depict $F_{535\ nm}/F_{485\ nm}$ (*A*) or $F_{485\ nm}/F_{535\ nm}$ (*B*) emission ratios in all observed biosensor-positive NMJ regions. Ratios were normalized to basal value before stimulation. Arrows indicate time points of lumbar stimulation. Mean ± SEM (n values with stimulation: 5 in *A*, 3 in *B*; n values without stimulation: 4 in *A*, 4 in *B*; $^*P < 0.05$, $^{**}P < 0.01$). (*C*) Quantification of nuclear accumulation of PPARGC1A-GFP upon sympathetic stimulation. Arrows indicate time points of lumbar stimulation. Mean ± SEM (n = 5; $^*P < 0.05$, $^{**}P < 0.01$).

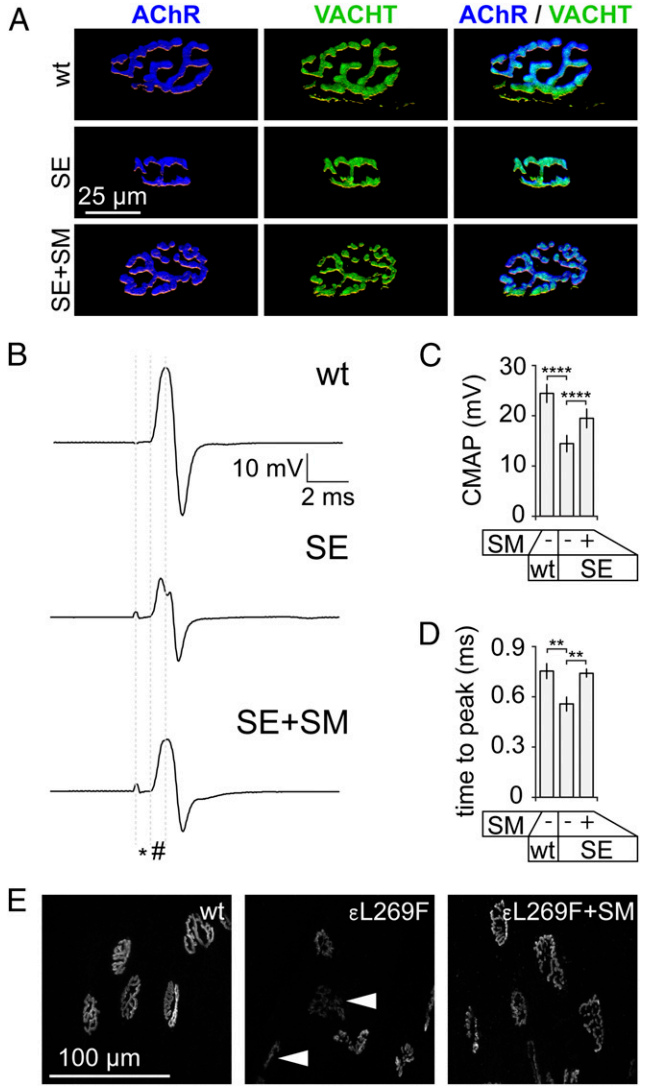

Fig. 3. SM treatment rescues NMJ phenotypes of sympathectomized muscle. (*A–D*) TA muscles of wild-type mice received injections of saline (wt) or 6-hydroxydopamine (SE) on alternate days for 2 wk. In the last 10 d, one SE group was also treated with s.c. daily doses of the SM clenbuterol (SE+SM). Then, muscles were harvested for IF (*A*) or CMAP recordings were made (*B–D*). (*A*) Muscles were taken and longitudinal sections were made and stained with BGT-AF555 and anti-VACHT antibody. Confocal microscopy was performed, signals were segmented, and 3D projections were calculated. Images show projections of representative NMJs. (*B–D*) In vivo CMAPs were recorded from TA muscles. Maximal stimuli of 0.25-ms duration were applied by a shielded microelectrode to the sciatic nerve. CMAP recordings used intramuscular needle electrodes. (*B*) Curves depict representative CMAPs from muscles treated as indicated. Latency (*), time to peak (#), and amplitude of CMAPs were determined. (*C*) Quantitative analysis revealed a significant reduction of CMAP amplitudes upon SE and partial rescue by SM. Mean ± SEM ($n = 8$, 5, and 5 for wt, SE, and SE+SM, respectively; $^{****}P < 0.0001$). (*D*) Quantitative analysis revealed a significant reduction of time to peak upon SE and full rescue by SM. Mean ± SEM ($n = 6$, 5, and 5 for wt, SE, and SE+SM, respectively; $^{**}P < 0.01$). (*E*) TA muscles of wild-type and myasthenic slow-channel *CHRNE L269F* mice (εL269F) received s.c. daily doses of saline or the SM clenbuterol for 10 d. At the start of s.c. treatments, NMJs were labeled with BGT-AF647. At the end of the treatment period, NMJs were imaged with in vivo confocal microscopy. Maximum z projections showing representative NMJs under the conditions indicated in the images: wt, wild type treated with saline; εL269F, εL269F treated with saline; εL269F+SM, εL269F treated with clenbuterol.

biosensor β2-AR-s-pep (19), which accumulated at the NMJ (Fig. S3 *C* and *D*). In vivo FRET imaging in combination with direct electrical stimulation of the sympathetic chain revealed a fast, sympathetic stimulation-dependent increase in postsynaptic ADRB2 activity (Fig. 2*A* and Fig. S3*E*). Next, to monitor postsynaptic cAMP production, a NMJ-specific cAMP sensor, termed "RAPSN-EPAC," was designed (Fig. S4). RAPSN-EPAC, which is composed of the receptor-associated protein of the synapse (RAPSN) followed by the cAMP-binding domains of the Exchange protein directly activated by cAMP (EPAC), showed specific localization at NMJs (Fig. S4*B*). In vivo imaging of RAPSN-EPAC demonstrated a consistent increase in postsynaptic cAMP levels upon direct stimulation of the sympathetic chain (Fig. 2*B* and Fig. S4*D*).

Given the recent success of SM in CMS treatment, we next tested the effect of the SM clenbuterol on AChRα1 subunit gene (CHRNA1) activity. Clenbuterol was applied s.c. daily for 10 d. Then, the amounts of CHRNA1 mRNA were determined from harvested muscles, showing a 10.23 ± 2.0-fold increase (mean ± SEM, $n = 4$; $P = 0.009$) in SM-treated muscles compared with saline-injected controls. Given that ADRB2 activation enhances expression of peroxisome proliferator-activated receptor γ-coactivator 1α (PPARGC1A) (20) and that PPARGC1A regulates NMJ-specific genes, including CHRNA1, in an activity-dependent manner (21), we addressed the effect of sympathetic chain stimulation on cytoplasm-to-nucleus shuttling of PPARGC1A. PPARGC1A-GFP was expressed in tibialis anterior (TA) muscles, and its amount in myonuclei upon stimulation of the sympathetic chain was observed by in vivo imaging. This revealed a rapid increase of PPARGC1A-GFP in myonuclei upon sympathetic chain stimulation (Fig. 2*C* and Fig. S5).

Effects of Sympathectomy and Rescue by Sympathicomimetics on NMJs. To address a trophic function of sympathetic input for the NMJ, we monitored NMJ morphology in the presence or absence of chemical sympathectomy (SE) by 6-hydroxydopamine (22, 23). As determined by IF, SE led to diminished complexity and size of NMJs (Fig. 3*A*). Quantitative analysis revealed a size reduction of NMJs upon SE compared with controls by 57 ± 5% (mean ± SEM, $n = 10$). Colocalization of pre- and postsynaptic structures remained unaffected under this condition and clenbuterol rescued the SE-induced effects (Fig. 3*A*), suggesting that they were due to lack of sympathetic activity rather than unspecific toxicity of 6-hydroxydopamine. Next, in vivo compound muscle action potentials (CMAPs) were obtained from TA muscles that were pretreated with SE and SM as just described. CMAPs from TA muscles were measured using intramuscular needle electrodes upon repetitive maximal sciatic nerve stimulation. Whereas latency (Fig. 3*B*, *) was unaltered in all conditions, amplitude and time to peak (Fig. 3*B*, #) of CMAPs were affected upon SE (Fig. 3 *B–D*). SM recovered the effects of SE on amplitude partially (Fig. 3*C*) and on time to peak completely (Fig. 3*D*).

The efficacy of SM for many CMS patients has been proven (3, 4). Here we used a myasthenic *CHRNE L269F* mouse model to test the effects of SM on NMJ morphology. AChRs were labeled with BGT. Then, mice received either saline or clenbuterol for 10 d. In vivo imaging of TA muscles was performed to reveal NMJ morphology. Similar to SE-treated wild-type mice (Fig. 3*A*), saline-treated myasthenic animals had aberrant NMJs with reduced size and complexity and weak BGT staining, indicating a diminished presence of AChRs. Due to scarce amounts of AChRs, many NMJs were hardly visible (Fig. 3*E*, *Center*, arrowheads). Conversely, NMJs of SM-treated *CHRNE L269F* mice looked largely normal (Fig. 3*E*). Compared with wild-type synapses, myasthenic NMJs were 44 ± 3% (mean ± SEM, $n = 6$; $P = 0.003$) smaller upon saline treatment but only 6 ± 14% (mean ± SEM, $n = 6$; $P = 0.36$) smaller upon clenbuterol application.

Discussion

This study addresses the distribution and functions of sympathetic neurons in skeletal muscle with several approaches. It reveals that sympathetic neurons innervate most NMJs in skeletal muscles, and that this innervation is crucial for synaptic integrity

and function. At this moment it cannot be concluded whether the stimulation of sympathetic neurons acts directly on skeletal muscle or indirectly via nearby blood vessels, motor neurons, or other cells. However, the sympathetic activation effect on cAMP signaling is consistent with a trophic function of sympathetic input for NMJs. The data corroborate the antagonistic activity of SE and SM with respect to expression of AChR. Previous studies have shown that a cAMP/PKA microdomain at the NMJ is important for synapse maintenance (24–28). Sympathetic input at NMJs is a candidate for maintaining this microdomain. The observed import of PPARGC1A into myonuclei upon sympathetic nerve stimulation is consistent with the transcriptional changes by SM postexercise (29). Because PPARGC1A is crucial in mitochondrial biogenesis (30), reduced mitochondrial protein synthesis postexercise after treatment with beta-blockers (31) could be explained as well. Because sympathetic input to skeletal muscles is via the sciatic nerve, various effects using sciatic denervation as an atrophy model might also have a sympathetic contribution. Fittingly, ganglionic sympathectomy increases proteolysis in rat muscles and norepinephrine treatment of denervated rat muscles reduces mRNA levels of the atrogenes MAFbx (syn. atrogin-1) and TRIM63 (syn. MuRF1) (2).

Future studies need to investigate whether sympathetic neurons form synaptic contacts with the NMJs or abut their neurotransmitters more distantly. Both options might be equally functional. As known from autonomous innervation of the central nervous system, monoamines, such as norepinephrine, can be distributed by volume transmission to reach several targets (32, 33). A general modulatory role of muscle function by sympathetic tone would benefit from an organization as a nerve net that elicits effects on several tissue components. This could harmonize muscle function and local circulation similar to respiratory–cardiovascular coupling (34).

Our findings provide a possible link to the success of SM in treating CMSs, and may help to explain phenomena of muscle weakness in many autonomous nervous system disorders. It remains to be studied whether SM primarily improves sarcomeric function, neuromuscular transmission, or a mixture of both. Although SM is effective in some forms of myasthenic syndromes (NMJ pathology) (3, 35–37) and spinal muscular atrophy (motor neuron defect involving the NMJ) (38), it was not effective in a trial for facioscapulohumeral muscular dystrophy (primary muscle pathology) (39). In clinics, sympathectomy is used to treat hyperhidrosis. Although sympathectomy is not reported to induce severe muscle weakness in patients, changes in muscle metabolism have been documented (40). Also, sympathectomy in rabbits evoked muscle atrophy and fiber splitting (40). Our experiments involving sympathectomy and SM treatment led to atrophy and its recovery, respectively (Fig. S6). Given the intimate relationship between synaptic function, muscle activity, and muscle trophicity, it is unlikely that these factors can be fully separated. However, the effects of beta-blockers on muscle fatigue (14) and anesthesia (15) suggest that an important component of sympathetic activity affects synaptic integrity and function.

The data presented here are consistent with a model where sympathetic neurons coinnervate several targets in muscle, including blood vessels, motor neurons, muscle fibers, and NMJs (Fig. S7). Complex cross-talk between these cell types might occur using feedback mechanisms that need to be addressed further. Sympathetic innervation controls muscle metabolism as well as maintenance and function of NMJs. The success of SM treatment of several forms of myasthenic syndromes should spur further elucidation of the involved signaling pathways to develop more selective and potent therapies.

Materials and Methods

Animals. All animals were kept and treated according to guidelines of the Brazilian College of Animal Experimentation and EU Directive 2010/63/EU. Experimental protocols were approved by the commission of ethics in animal research of the School of Medicine of Ribeirão Preto and national authorities in France, Germany, and the United Kingdom. Adult male and female C57BL/10J, CHRNE L269F, B6.Cg-Gt(ROSA)26Sor$^{tm9(CAG\text{-}tdTomato)Hze}$/J x B6-Tg(DBH-iCre) (called DBH-Tomato) were used for experiments. Anesthesia and preparation of mice for microscopy and electrophysiology were performed as described (25).

Immunofluorescence and Molecular Biosensors. IF stainings of diaphragm, muscle cross-sections, and EDL longitudinal sections are described in Figs. S1–S3. EDL and soleus were used as paradigms for fast and slow muscles, respectively, diaphragm for its band-like array of NMJs, and TA for electroporation because of its in vivo accessibility. Molecular biosensors and their transfection are described in Figs. S3–S5.

Microscopy and Image Analysis. All microscopy used a DMRE TCS SP2 confocal and two-photon microscope equipped with Leica Confocal Software 2.61, a KrAr laser (488 nm, 514 nm), a diode-pumped laser (561 nm), an HeNe laser (633 nm), a tunable Mai Tai pulsed two-photon laser, and a 63×/1.2 NA HCX PL APO CS water immersion objective for fixed samples as well as 20×/0.7 N. A. HC PL APO CS IMM/CORR UV and 63×/1.2 N.A. HCX PL APO CS W CORR objectives (all Leica Microsystems) for in vivo imaging (immersion medium, Visc-Ophtal gel; Dr. Winzer Pharma). For further details regarding microscopy of fixed samples, in vivo imaging, and image analysis, see Figs. S1 and S3. Image composition used Photoshop and Illustrator (Adobe Systems Software).

Sciatic Denervation, Stimulation of Lumbar Sympathetic Ganglionic Chain, and Pharmacological Treatments. Sciatic denervation was as described (41). For details regarding the stimulation of the sympathetic ganglionic chain, see Fig. S3. Clenbuterol solution in PBS was always freshly prepared and then injected s.c. (3 mg/kg) for 10 d before microscopy. Chemical sympathectomy used 6-hydroxydopamine (22) (in 0.3% ascorbic acid oxygen-free water), which was injected into hindlimbs (100 mg/kg) on alternate days for 2 wk before imaging.

Compound Muscle Action Potential Measurement. Mice were kept under isoflurane anesthesia. CMAP measurements were performed after saline, SE, or SE+SM treatment (Fig. 3 *B–D*) with maximal electrical stimulations delivered by a microelectrode (Harvard Apparatus) to the sciatic nerve. An A.M.P.I. Master-8-cp stimulator provided pulses at 0.25-ms duration and 5-Hz frequency. CMAPs were recorded by needle electrodes connected to a Bio Amp and a PowerLab 8/35 running LabChart 8 software (ADInstruments). Data analysis used LabChart 8 and Microsoft Excel:mac2011.

Statistical Analysis. Graphic representation of data used Microsoft Excel: mac2011 and Adobe Illustrator. Significance was tested with Student *t* test or Welch test, where applicable. Kolmogorov–Smirnov test for normal distribution and *F* test for homo/heteroscedasticity were performed. Sample sizes were calculated to reach 80% power and $\beta < 0.2$.

ACKNOWLEDGMENTS. We thank Dr. Steve Laval for critical discussions, and acknowledge the help of animal facilities at the host institutes. T.P. was funded by the National Research Council (CNR) Special Project "Bioimaging." S.L. and R.R. were supported by European Commission International Research Staff Exchange Scheme (IRSES) Grant SarcoSi, Deutsche Forschungsgemeinschaft (DFG) Grants La668/15-1, RU923/7-1, and RU923/8-1, and a grant from Hector Stiftung. H.L. is supported by Medical Research Council (MRC) UK (Reference G1002274, Grant 98482) and by the European Commission (FP7/2007-2013) under Grant Agreements 305444 (RD-Connect) and 305121 (Neuromics). D. Lustrino, W.A.S., I.C.K., and L.C.C.N. were funded by Sao Paolo Research Foundation (FAPESP) (2012/51456-1; 2012/24524-6; 2012/05697-7; 2010/11083-6).

1. Barker D, Saito M (1981) Autonomic innervation of receptors and muscle fibres in cat skeletal muscle. *Proc R Soc Lond B Biol Sci* 212(1188):317–332.
2. Silveira WA, et al. (2014) Activating cAMP/PKA signaling in skeletal muscle suppresses the ubiquitin-proteasome-dependent proteolysis: Implications for sympathetic regulation. *J Appl Physiol* 117(1):11–19.
3. Rodríguez Cruz PM, Palace J, Beeson D (2014) Congenital myasthenic syndromes and the neuromuscular junction. *Curr Opin Neurol* 27(5):566–575.
4. Engel AG, Shen X-M, Selcen D, Sine SM (2015) Congenital myasthenic syndromes: Pathogenesis, diagnosis, and treatment. *Lancet Neurol* 14(4):420–434.
5. Okamoto LE, Raj SR, Biaggioni I (2012) Chronic fatigue syndrome and the autonomic nervous system. *Primer on the Autonomic Nervous System*, eds Robertson D, Biaggioni I, Burnstock G, Low PA, Paton JFR (Academic, Amsterdam), 3rd Ed, pp 531–534.
6. Tachi N, Ohya K, Chiba S, Nihira H, Minagawa K (1995) Muscle involvement in congenital insensitivity to pain with anhidrosis. *Pediatr Neurol* 12(3):264–266.

7. Munver R, Volfson IA (2006) Adrenal insufficiency: Diagnosis and management. *Curr Urol Rep* 7(1):80–85.
8. Trikudanathan S, Williams GH (2012) Altered adrenal function and the autonomic nervous system. *Primer on the Autonomic Nervous System*, eds Robertson D, Biaggioni I, Burnstock G, Low PA, Paton JFR (Academic, Amsterdam), 3rd Ed, pp 571–574.
9. Jänig W (2012) Complex regional pain syndrome. *Primer on the Autonomic Nervous System*, eds Robertson D, Biaggioni I, Burnstock G, Low PA, Paton JFR (Academic, Amsterdam), 3rd Ed, pp 583–587.
10. Jänig W (2010) The fascination of complex regional pain syndrome. *Exp Neurol* 221(1):1–4.
11. Titulaer MJ, Lang B, Verschuuren JJ (2011) Lambert-Eaton myasthenic syndrome: From clinical characteristics to therapeutic strategies. *Lancet Neurol* 10(12): 1098–1107.
12. Morgan-Followell B, de Los Reyes E (2013) Child neurology: Diagnosis of Lambert-Eaton myasthenic syndrome in children. *Neurology* 80(21):e220–e222.
13. Khurana RK (2012) Paraneoplastic autonomic dysfunction. *Primer on the Autonomic Nervous System*, eds Robertson D, Biaggioni I, Burnstock G, Low RA, Paton JFR (Academic, Amsterdam), 3rd Ed, pp 593–596.
14. Hunter AM, et al. (2002) The effect of selective beta1-blockade on EMG signal characteristics during progressive endurance exercise. *Eur J Appl Physiol* 88(3): 275–281.
15. Kim KS, Kim KH, Shin WJ, Yoo HK (1998) Neuromuscular interactions between mivacurium and esmolol in rabbits. *Anaesthesia* 53(2):140–145.
16. Stanke M, et al. (2006) Target-dependent specification of the neurotransmitter phenotype: Cholinergic differentiation of sympathetic neurons is mediated in vivo by gp 130 signaling. *Development* 133(1):141–150.
17. Kim YS, Sainz RD, Molenaar P, Summers RJ (1991) Characterization of beta 1- and beta 2-adrenoceptors in rat skeletal muscles. *Biochem Pharmacol* 42(9):1783–1789.
18. Williams RS, Caron MG, Daniel K (1984) Skeletal muscle beta-adrenergic receptors: Variations due to fiber type and training. *Am J Physiol* 246(2 Pt 1):E160–E167.
19. Malik RU, et al. (2013) Detection of G protein-selective G protein-coupled receptor (GPCR) conformations in live cells. *J Biol Chem* 288(24):17167–17178.
20. Miura S, et al. (2007) An increase in murine skeletal muscle peroxisome proliferator-activated receptor-gamma coactivator-1alpha (PGC-1alpha) mRNA in response to exercise is mediated by beta-adrenergic receptor activation. *Endocrinology* 148(7): 3441–3448.
21. Handschin C, et al. (2007) PGC-1alpha regulates the neuromuscular junction program and ameliorates Duchenne muscular dystrophy. *Genes Dev* 21(7):770–783.
22. Thoenen H, Tranzer JP (1968) Chemical sympathectomy by selective destruction of adrenergic nerve endings with 6-hydroxydopamine. *Naunyn Schmiedebergs Arch Exp Pathol Pharmakol* 261(3):271–288.
23. Picklo MJ (1997) Methods of sympathetic degeneration and alteration. *J Auton Nerv Syst* 62(3):111–125.
24. Röder IV, et al. (2010) Myosin Va cooperates with PKA RIalpha to mediate maintenance of the endplate in vivo. *Proc Natl Acad Sci USA* 107(5):2031–2036.
25. Choi K-R, et al. (2012) Rapsyn mediates subsynaptic anchoring of PKA type I and stabilisation of acetylcholine receptor in vivo. *J Cell Sci* 125(Pt 3):714–723.
26. Röder IV, et al. (2012) Participation of myosin Va and Pka type I in the regeneration of neuromuscular junctions. *PLoS One* 7(7):e40860.
27. Nelson PG, Lanuza MA, Jia M, Li MX, Tomas J (2003) Phosphorylation reactions in activity-dependent synapse modification at the neuromuscular junction during development. *J Neurocytol* 32(5-8):803–816.
28. Martinez-Pena y Valenzuela I, Pires-Oliveira M, Akaaboune M, Akaaboune M (2013) PKC and PKA regulate AChR dynamics at the neuromuscular junction of living mice. *PLoS One* 8(11):e81311.
29. Bruno NE, et al. (2014) Creb coactivators direct anabolic responses and enhance performance of skeletal muscle. *EMBO J* 33(9):1027–1043.
30. Geng T, et al. (2010) PGC-1alpha plays a functional role in exercise-induced mitochondrial biogenesis and angiogenesis but not fiber-type transformation in mouse skeletal muscle. *Am J Physiol Cell Physiol* 298(3):C572–C579.
31. Robinson MM, Bell C, Peelor FF, III, Miller BF (2011) Beta-adrenergic receptor blockade blunts postexercise skeletal muscle mitochondrial protein synthesis rates in humans. *Am J Physiol Regul Integr Comp Physiol* 301(2):R327–R334.
32. Agnati LF, et al. (1986) A correlation analysis of the regional distribution of central enkephalin and beta-endorphin immunoreactive terminals and of opiate receptors in adult and old male rats. Evidence for the existence of two main types of communication in the central nervous system: The volume transmission and the wiring transmission. *Acta Physiol Scand* 128(2):201–207.
33. Fuxe K, et al. (2012) Extrasynaptic neurotransmission in the modulation of brain function. Focus on the striatal neuronal-glial networks. *Front Physiol* 3:136.
34. Anrep GV, Pascual W, Rössler R (1936) Respiratory variations of the heart rate. II. The central mechanism of the sinus arrhythmia and the inter-relationship between central and reflex mechanism. *Proc R Soc Lond B Biol Sci* 119:218–230.
35. Liewluck T, Selcen D, Engel AG (2011) Beneficial effects of albuterol in congenital endplate acetylcholinesterase deficiency and Dok-7 myasthenia. *Muscle Nerve* 44(5): 789–794.
36. Burke G, et al. (2013) Salbutamol benefits children with congenital myasthenic syndrome due to DOK7 mutations. *Neuromuscul Disord* 23(2):170–175.
37. Schara U, et al. (2009) Ephedrine therapy in eight patients with congenital myasthenic syndrome due to DOK7 mutations. *Neuromuscul Disord* 19(12):828–832.
38. Pane M, et al. (2008) Daily salbutamol in young patients with SMA type II. *Neuromuscul Disord* 18(7):536–540.
39. Kissel JT, et al.; FSH-DY Group (2001) Randomized, double-blind, placebo-controlled trial of albuterol in facioscapulohumeral dystrophy. *Neurology* 57(8):1434–1440.
40. Hashmonai M, Kopelman D (2003) The pathophysiology of cervical and upper thoracic sympathetic surgery. *Clin Auton Res* 13(Suppl 1):I40–I44.
41. Strack S, et al. (2011) A novel labeling approach identifies three stability levels of acetylcholine receptors in the mouse neuromuscular junction in vivo. *PLoS One* 6(6): e20524.
42. Renier N, et al. (2014) iDISCO: A simple, rapid method to immunolabel large tissue samples for volume imaging. *Cell* 159(4):896–910.
43. Röder IV, et al. (2008) Role of myosin Va in the plasticity of the vertebrate neuromuscular junction in vivo. *PLoS One* 3(12):e3871.
44. Rudolf R, Hafner M, Mongillo M (2012) Investigating second messenger signaling in vivo. *Methods Enzymol* 505:363–382.
45. Nikolaev VO, Bünemann M, Hein L, Hannawacker A, Lohse MJ (2004) Novel single chain cAMP sensors for receptor-induced signal propagation. *J Biol Chem* 279(36): 37215–37218.
46. Puigserver P, et al. (1998) A cold-inducible coactivator of nuclear receptors linked to adaptive thermogenesis. *Cell* 92(6):829–839.